Acta Pharmaceutica Sinica B 2022;12(4):1987−1999

Chinese Pharmaceutical Association
Institute of Materia Medica, Chinese Academy of Medical Sciences

Acta Pharmaceutica Sinica B

www.elsevier.com/locate/apsb
www.sciencedirect.com

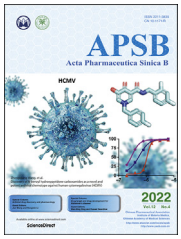

ORIGINAL ARTICLE

Intelligent lesion blood−brain barrier targeting nano-missiles for Alzheimer's disease treatment by anti-neuroinflammation and neuroprotection

Xueqin He[a,†], Xiaorong Wang[a,†], Lianyi Yang[a], Zhihang Yang[a], Wenqi Yu[a], Yazhen Wang[a], Rui Liu[a], Meiwan Chen[b], Huile Gao[a,*]

[a]*Key Laboratory of Drug-Targeting and Drug Delivery System of the Education Ministry and Sichuan Province, Sichuan Engineering Laboratory for Plant-Sourced Drug and Sichuan Research Center for Drug Precision Industrial Technology, West China School of Pharmacy, Sichuan University, Chengdu 610041, China*
[b]*State Key Laboratory of Quality Research in Chinese Medicine, Institute of Chinese Medical Sciences, University of Macau, Macau 999078, China*

Received 18 November 2021; received in revised form 14 December 2021; accepted 10 January 2022

KEY WORDS

Receptor for advanced glycation end products;
ROS-responsive;
Blood–brain barrier transcytosis;
Alzheimer's disease;
Drug combination;
Anti-neuroinflammation;
Neuroprotection;
Nano drug delivery system

Abstract The treatment of Alzheimer's disease (AD) is one of the most difficult challenges in neurodegenerative diseases due to the insufficient blood–brain barrier (BBB) permeability and unsatisfactory intra-brain distribution of drugs. Therefore, we established an ibuprofen and FK506 encapsulated drug co-delivery system (Ibu&FK@RNPs), which can target the receptor of advanced glycation endproducts (RAGE) and response to the high level of reactive oxygen species (ROS) in AD. RAGE is highly and specifically expressed on the lesion neurovascular unit of AD, this property helps to improve targeting specificity of the system and reduce unselective distribution in normal brain. Meanwhile, these two drugs can be specifically released in astrocytes of AD lesion in response to high levels of ROS. As a result, the cognition of AD mice was significantly improved and the quantity of Aβ plaques was decreased. Neurotoxicity was also alleviated with structural regeneration and functional recovery of neurons. Besides, the neuroinflammation dominated by NF-κB pathway was significantly inhibited with decreased NF-κB and IL-1β in the brain. Overall, Ibu&FK@RNPs can efficiently and successively target diseased BBB and astrocytes in AD lesion. Thus it significantly enhances intracephalic accumulation of drugs and efficiently treats AD by anti-neuroinflammation and neuroprotection.

*Corresponding author.
E-mail addresses: gaohuile@scu.edu.cn, gaohuilescu@163.com (Huile Gao).
[†]These authors made equal contributions to this work.

Peer review under responsibility of Chinese Pharmaceutical Association and Institute of Materia Medica, Chinese Academy of Medical Sciences

https://doi.org/10.1016/j.apsb.2022.02.001

1. Introduction

Alzheimer's disease (AD), one of the most challengeable neurodegenerative diseases, is characterized by progressive cognitive dysfunction and behavioral impairment occurring in old and pre-old age[1]. However, there were only five available medicines before 2021[2], so it is urgent to find effective therapeutic targets and develop efficacious pharmaceutical preparations. The mainstream direction of AD researches is β amyloid (Aβ) cascade hypothesis, but all clinical trials were interrupted due to the lack of damaged neuronal recovery[2–4]. Alternatively, there emerged other therapeutic targets of AD, including microtubule-associated protein, anti-neuroinflammation, synaptic and neuroprotection, metabolism, neurogenesis, vascular system and epigenetic drugs, among which the number of anti-neuroinflammatory and neuroprotective drugs has fastest growing[5]. Besides, more and more researches have shown the comprehensive effects of multiple pathogenic mechanisms in AD, showing the common feature of neuroinflammatory microenvironment[6].

Neuroinflammation, characterized by excessively activated glial cells and overexpressed inflammatory factors in AD, can interact with neurons and lead to protein deposition and neuronal dysfunction[6–9]. The corresponding neuronal responses will conversely stimulate inflammation to form a vicious circle and aggravate AD[10]. Therefore, it would be effective by using anti-neuroinflammatory treatment to undermine the positive feedback loop of neuroinflammation and neuronal dysfunction. Nuclear factor kappa B (NF-κB) pathway mainly exists in excessively activated astrocytes of neurodegenerative diseases, and it plays an important role in anti-neuroinflammatory mechanisms[6–9]. Nonsteroidal anti-inflammatory drugs (NSAIDs) are most widely used drugs in inhibiting NF-κB signaling pathway[11–17], and high-dose of ibuprofen have been confirmed to improve dementia-like symptoms in AD animal models[18–20]. Moreover, ibuprofen can normalize the microenvironment of the lesion to stop disease deterioration. But it can't make neuronal damages reversed to cure AD completely. So it is necessary to use neuroprotective drugs additionally. Calcineurin inhibitor (tacrolimus, FK506), the most effective neuroprotective drug in central nervous system diseases, can maintain intracellular calcium homeostasis to improve neuronal repair and regeneration[21–26]. Moreover, the amelioration of AD-like behavior has been observed in patients taking FK506[21,24,26]. To sum up, we combined ibuprofen and FK506 for AD treatment, which could not only inhibit neuroinflammation mediated by NF-κB pathway, but also exert neuroprotective effects.

For brain targeted drug delivery, the blood–brain barrier (BBB), which is composed by dense endothelial cells and supported by multiple cells, greatly restricts their internalization and transportation[27–29]. To overcome BBB, receptor-mediated transport (CMT) is the most widely used strategy in nano-targeted delivery systems[27,30]. However, traditional CMT-based brain targeting delivery leads to unselective distribution in whole brain because of the homogenous expression of targeted receptors on BBB[31]. It is important to find targets that are restrictively expressed on BBB of lesion[32]. In AD lesion sites, the receptor of advanced glycation endproducts (RAGE) is specifically and highly expressed on the diseased neurovascular unit, including cerebral vascular endothelial cells, astrocytes and neurons[33–37]. RAP peptide (sequence: CELKVLMEKEL) is a specific ligand of RAGE, which could assist with the transportation of nanoparticles into diseased brain parenchyma through CMT[38]. Furthermore, microenvironment responsive drug delivery systems could be introduced to achieve rapid and responsive drug release in the lesion and reduce undemand drug leakage in healthy areas[39–41]. In view of the high level of reactive oxygen species (ROS) in AD[42,43], ROS-sensitive thioether bond (MAH-EDT) was introduced into nanoparticles, which would be broken when exposed in ROS, inducing nanoparticles decomposition and drug release[44,45]. Eventually, the ROS-responsive RAGE-targeted drug delivery system was established for ibuprofen and FK506 delivery.

In this study, we developed an ROS-responsive and RAGE-targeted drug delivery platform (Ibu&FK@RNPs). The ROS-sensitive sulfur ether linker (MAH-EDT) was used to link polycaprolactone (PCL) and poly(ethylene glycol) (PEG) with RAP-modified at PEG-terminus, and then self-assembled into nanoparticles with ibuprofen and FK506 encapsulated (Fig. 1A). With the assistance of RAP, Ibu&FK@RNPs targeted RAGE on diseased BBB and was transported into targets cells by CMT. After reaching the AD lesion and exposed in the high level of ROS, Ibu&FK@RNPs collapsed and instantaneously released ibuprofen and FK506 to treat AD (Fig. 1B). As a result, the cognition of AD mice was significantly improved and the production of Aβ plaques was inhibited. Neurotoxicity induced by calcium homeostasis imbalance was also alleviated and the neuroinflammatory response was significantly inhibited. Overall, this system successively targeted the BBB in AD lesion, astrocytes and neurons, thus significantly enhancing the intracephalic drug accumulation and treatment efficacy.

2. Materials and methods

2.1. Reagents, synthesis and characterization

MPEG-PCL (M_n = 3400:15,000) and FITC-PEG-PCL (M_n = 3400:15,000) were provided by Prof. Jianyuan Hao (University of Electronic Science and Technology of China, chengdu, China). RAP (sequence: CELKVLMEKEL) was synthesized by Sangon Biotech Co., Ltd. (Shanghai, China). Aβ_{1-42} was purchased from GL Biochem Ltd. (Shanghai, China). Maleimide (MAL) functionalized polyethylene glycol (MAL-PEG-MAL, M_n = 3500) was purchased from Jenkem Technology Co., Ltd. (Beijing, China). The MAP2 antibody, HRP goat anti-rabbit IgG (H+L), β-actin rabbit mAb and FITC goat anti-rabbit IgG (H+L) were purchased from Abclonal (China). Anti-Aβ_{1-42} antibody, anti-IκBα and GFAP antibody were purchased from Abcam (USA). The NF-κB p65 rabbit mAb was purchased from CST (USA). The mouse IL-1β valukine ELISA was purchased from Novus (USA). The goat serum and PMSF were purchased from Solarbio (China). The Cell lysis buffer for Western and IP was purchased from Beyotime (China). Dulbecco's modified Eagle's medium (DMEM), trypsin-EDTA solutions and FBS were purchased from Gibco (USA). The bEnd.3 and PC12 cell lines were obtained from the Chinese Academy of Sciences Cell Bank (Shanghai, China). Other chemicals were analytical or reagent grade.

2.1.1. Synthesis of ROS-sensitive linker (EDT-MAA)

The ROS-labile sulfur ether cross linker was synthesized according to the published methods[45,46]. Briefly, 1,2-ethanedithiol (1.049 mL, 12.5 mmol, 1 eq.) and 1,1-dimethylethyl methacrylate (2.031 mL, 12.5 mmol, 1 eq.) were added into a 10 mL round bottom flask. And then triethylamine (15.4 μL, 0.5%, *v/v*) was dropped slowly into the mixture. After stirred for 12 h at room

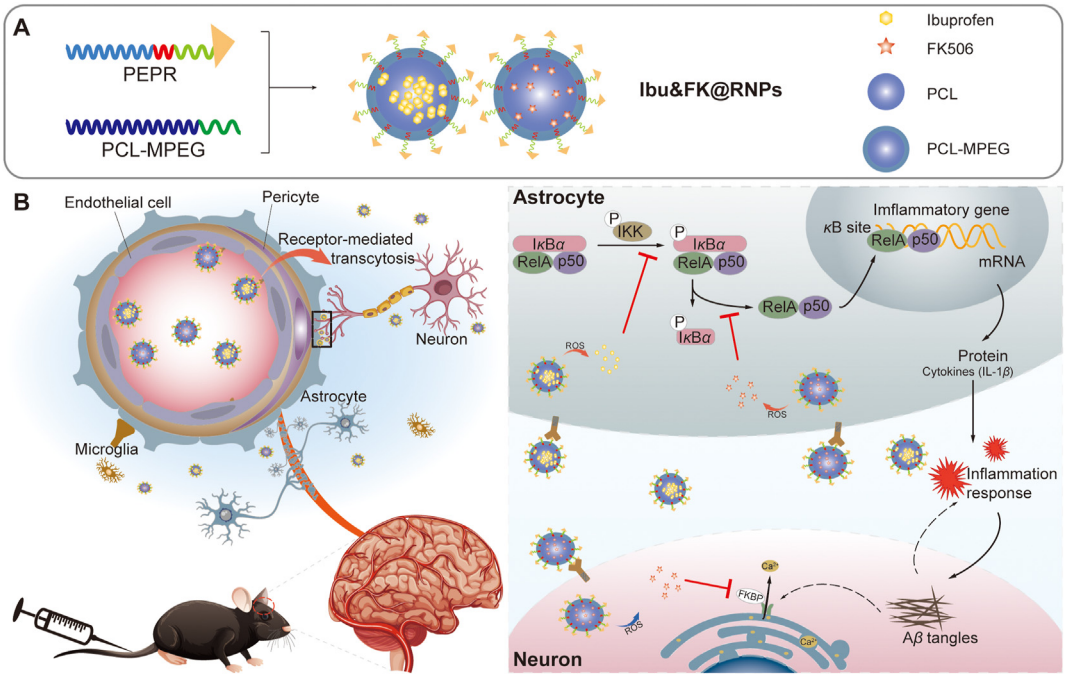

Figure 1 (A) Diagram depicting the preparation of ROS-responsive programmed RAGE-targeted delivery depot of Ibu&FK@RNPs. (B) Schematic illustration of Ibu&FK@RNPs target RAGE on lesion BBB and brain parenchymal cells. Amplification: schematic diagram of process of the ROS-responsive drug release from nanoparticles in astrocytes and neurons, and then treat AD by anti-neuroinflammation and neuroprotection.

temperature, the product (compound **1**) was detected by UV thin-layer chromatography plates.

2.1.2. Synthesis of polycaprolactone (PCL)

PCL was synthesized according to a previous study[47]. At first, calcium hydride (457.8 mg) and *ε*-caprolactone (15 mL) were added into a round bottom flask and distilled under reduced pressure to obtain dry *ε*-caprolactone. And then, dry *ε*-caprolactone (2.77 mL), benzyl alcohol (129.2 μL) and stannous isooctanoate (22.7 μL) were added into a 50 mL round bottom flask. After stirred for 24 h at 120 °C under the protection of argon, the products were cooled down to room temperature. At last, the reaction solid was dissolved into dichloromethane (15 mL) and precipitated by dropwise adding to methanol. After repeated for 3 times, the precipitated powder was collected and recrystallized for 3 times to yield the PCL.

2.1.3. Synthesis of ROS-sensitive cleavable MAL-PEG-EDT-MAA (PEP)

Synthesis of MAL-PEG-EDT-MAA: Compound **1** (1.54 μL, 6.25 nmol, 1 eq.), MAL-PEG$_{3500}$-MAL (32.8 mg, 9.34 nmol, 1.5 eq.) were dissolved into deionized water (3 mL), and triethylamine (15 μL, 0.5%, *v/v*) was added. After kept stirring for 12 h at room temperature, the reaction mixture was poured into deionized water (50 mL) and 1 mol/L hydrochloric acid was dropped slowly into the solution to neutralize the triethylamine. Then, the mixture was wash 3 times by hexane (100 mL) and extracted by dichloromethane (DCM) for 3 times. The reaction mixture was finally evaporated under vacuum to remove the organic solvent and the creamy yellow reaction product (compound **2**) was obtained.

2.1.4. Synthesis of PCL-MAH-EDT-PEG-MAL

Firstly, the synthesized compound **2** (9 mg) was deprotected by refluxing for 6 h with 1 mL trifluoroacetic acid in DCM (2 mL). The liquid was washed with sodium hydroxide solution and water 3 times and the DCM was finally evaporated and the white reaction product (compound **3**) was obtained. Then, PCL (1 mg), compound **3** (5 mg), DMAP (1 mg) and EDC (5 mg) were dissolved into dry DCM (3 mL). After stirred for 12 h at room temperature, the mixture was evaporated and then dissolved into dimethyl sulfoxide (DMSO, 2 mL) again. The liquid was collected after dialysis in DMSO and deionized water for 24 h, respectively using dialysis tube (3500 Da, Sigma−Aldrich, USA). After removed unreacted ingredients, the solution was lyophilized and the final product (compound **4**) was obtained.

2.1.5. Synthesis of RAGE targeting PEPR

The RAP peptide (5 mg) and compound **4** (20 mg) were dissolved into 3 mL acetone, and then triethylamine (15 μL) were added to maintain the alkaline environment. After continued stirring for 12 h at room temperature, the mixed solvent was evaporated and then dissolved into DMSO (2 mL) again. The mixture was collected after dialysis in DMSO and deionized water for 24 h, respectively using dialysis tube (3500 Da). After unreacted ingredients being removed, the solution was lyophilized and the final product was obtained.

2.1.6. Preparation of drug-loaded nanoparticles

To give an overall comparison, the ROS-sensitive and RAP-decorated PCL-PEG (PEPR), ROS-sensitive PCL-PEG without RAP decoration (PEP) and methoxyl PCL-PEG (PCL-MPEG) were prepared. Preparation of Ibuprofen@NPs: Ibuprofen

(5.94 mg), PCL-MPEG (127.8 mg) and PEP (4.83 mg) were dissolved in acetone (1 mL) and then mixed with deionized water (20 mL). With the magnetic stirring of 600 rpm, the Ibuprofen@NPs was formed. After 4 h of stirring, organic regents were removed *via* rotary evaporator. Ibuprofen@NPs was collected after centrifugation at 8000×*g* for 10 min. Preparation of Ibuprofen@RNPs: The Ibuprofen@RNPs was prepared as above, except that the PEPR (3.9 mg) was added into the solution rather than PEP. Preparation of FK506@NPs: A total of FK506 (0.36 mg), PCL-MPEG (3.2 mg) and PEP (0.1 mg) were dissolved in acetone (100 μL) and then mixed with deionized water (2 mL). With the magnetic stirring of 600 rpm, the FK506@NPs was formed. After 4 h of stirring, organic regents were removed *via* rotary evaporator. The FK506@NPs was collected after centrifugation at 8000×*g* for 10 min. Preparation of FK506@RNPs: The FK506@RNPs was prepared as above, except that the PEPR (0.11 mg) was added into the solution rather than PEP.

2.1.7. *Preparation of Cou6@NPs*

Coumarin-6 (Cou6, 0.6 μg), PCL-MPEG (2.576 mg) and PEP (0.079 mg) were dissolved in acetone (100 μL) and then mixed with deionized water (2 mL). With the magnetic stirring of 600 rpm, the Cou6@NPs was formed. After 4 h of stirring, organic regents were removed *via* rotary evaporator and the solution was purified by Sephadex G-25 (Aladdin, China). The Cou6@NPs was concentrated after ultrafiltration at 5000×*g* using Ultra-4 (Amicon, 100kD, Millipore, USA) concentrator tube to appropriate concentration. Preparation of Cou6@R_nNPs: The Cou6@R_nNPs was prepared as above and the formula as follows (Supporting Information Table S1).

2.1.8. *Characterization*

The particle size and zeta potential of the complexes were evaluated using the dynamic light scattering technique on a Malvern meter (Malvern, UK). The morphology was observed using a transmission electron microscope (TEM, H-600, Hitachi, Japan). The drug-loading capacity and encapsulation efficiency of ibuprofen and FK506 was measured by high performance liquid chromatography (Agilent LC-20A, Japan), which were referred to the standard of "*Chinese Pharmacopoeia*" (ChP, 2015 edition) and "Import standard for tacrolimus capsule sustained-release tablets" (TX20100019), respectively.

2.1.9. *Serum stability*

The plasma stability of different formulations was evaluated in PBS with different concentration of fetal bovine serum (FBS). Ibuprofen@NPs, Ibuprofen@RNPs, FK506@NPs and FK506@RNPs were suspended in water, PBS with 0%, 10% and 50% FBS and incubated under the condition of 75 rpm, 37 °C. The particle size was determined by dynamic light scattering.

2.2. *Studies in cells*

Quantified Fluorescence Intensity by Flow Cytometry: bEnd.3 cells were seeded at the density of 5×10^4 cells per well in 12-well plates and cultured at 37 °C for 24 h. For the mimetic environment of AD, 20 μmmol/L of Aβ oligomers (500 μL) were added into the well. The Cou6-labled nanoparticles (2.7 mg/mL of RNPs with 0.6 μg/mL of Coumarin-6) and cells were incubated together for 2 h at 37 °C. Then cells were washed 3 times with PBS buffer. The single cell suspension was prepared and quantified by flow cytometry (BD FACS Celesta, USA).

2.2.1. *Preparation of Aβ oligomers*

Aβ polymers were dissolved into hexafluoroisopropanol at the concentration of 5 mg/mL. After dissolved by ultrasound for 30 min, the mixture was incubated at 25 °C for 2 h. The faint yellow solid, subpackaged and dried with nitrogen, would be stored at −20 °C for stand-by use. A little aseptic DMSO could be involved and dissolved by ultrasound for 10 min. Before use, Aβ oligomers would be diluted by 10 mM PBS buffer to scheduled concentration.

2.2.2. *Screening the concentration of Aβ oligomers for inducing RAGE expression of cells*

After incubated with Aβ oligomers for 12 h, bEnd.3 and PC12 cells viability by MTT assays were applied to select the appropriate concentration.

2.2.3. *Cytotoxicity assay*

Cytotoxicity was assessed using an MTT assay. Briefly, bEnd.3 cells were grown on 96-well plates by the concentration of 5×10^3 cells/well. After 12 h, 20 μmol/L Aβ oligomers were dosed for 12 h and then different concentrations of drugs, empty nanoparticles and drug-loaded nanoparticles were incubated with the cells for 12 h. Subsequently, the MTT method was used to determine cell viability. Untreated cells were used as the negative controls, and the viability was expressed as the percentage of the absorbance of the negative control.

2.2.4. *Qualitative fluorescence intensity by confocal microscopy*

The same cell treated procedure was operated as the quantified analysis. After incubation, slides adhered cells were fixed with 4% paraformaldehyde for 30 min and then stained with 0.5 μg/mL DAPI for 5 min. Fluorescence intensity was observed with laser scanning confocal microscopy (Eclipse Ti, Nikon, Japan).

2.3. *Studies in animals*

The male BALB/c mice and C57BL/6 mice were purchased from Byrness Weil Biotech., Ltd. (Chongqing, China). APP/PS1 mice were purchased from the Cavens Laboratory Animal Co., Ltd. (Jiangsu, China). All animals were maintained under SPF grade feeding conditions and experiments were approved by the Animal Experimentation Ethics Committee of Sichuan University.

2.3.1. *Synthesis of Cy5.5-labled ibuprofen (Cy5.5-Ibu)*

Ibuprofen (2 mg), *N*,*N*′-dicyclohexylcarbodiimide (2 mg) and Cy5.5 amine (1 mg) were dissolved in dry DCM (6 mL) and then pH was adjusted to 8−9 by using *N*,*N*-diisopropylethylamine. The reaction mixture was then replaced under nitrogen to completely remove the oxygen. After string for 2 h in ice-water bath, the reactants were turned to room temperature and continued reacting for 12 h. The mixture was placed at 4 °C for the fully precipitation of insoluble components and the supernatant were collected after centrifugation at 10,000×*g* for 10 min. Organic regents were removed *via* rotary evaporator and solids were dissolved into DMSO (2 mL) again. The mixture was collected after dialysis in DMSO and deionized water for 24 h, respectively using dialysis tube (500 kDa). After removed unreacted ingredients, the solution was lyophilized and the final product was obtained.

2.3.2. *Preparation of Cy5.5-Ibu@NPs*

A total of Cy5.5-Ibu (2 mg), FITC-PCL-PEG (97 mg) and PEP (3 mg) were dissolved in acetone (2 mL) and then mixed with

deionized water (40 mL). With the magnetic stirring of 600 rpm, the Cy5.5-Ibu@NPs was formed. After 4 h of stirring, organic regents were removed *via* rotary evaporator and the solution was purified by Sephadex G-25 (Aladdin, China). The Cy5.5-Ibu@NPs was concentrated after ultrafiltration at 5000×*g* using Ultra-4 (Amicon, 100 kDa, Millipore, USA) concentrator tube to appropriate concentration.

2.3.3. *Preparation of Cy5.5-Ibu@RNPs*

The Cy5.5-Ibu@RNPs was prepared as above, except that PEPR (3.5 mg) was added into the solution except for PEP.

2.3.4. *In vivo imaging*

The AD mice were intravenously injected with Cy5.5-Ibu-labeled nanoparticles (1 mg/kg of Cy5.5-Ibu, equal to 50 mg/kg of RNPs). After injected for 1, 2, 4 and 6 h, mice were imaged using the Lumina III Imaging System (PerkinElmer, USA). At 6 h, the mice were sacrificed and their organs (heart, liver, spleen, lung, kidney and brain) were separated and captured as above. All tissues were totally soaked into 4% paraformaldehyde for 24 h, dehydrated with sucrose solution step by step and embedded in Tissue-Tek O.C.T compound (Sakura Finetek, USA). Then they were sectioned at 10 μm with the freezing microtome (Leica CM1950, Germany). Brain slides were operated by immunofluorescence of anti-RAGE antibody and other organs were stained with DAPI. The images of co-localization were observed using a confocal microscope.

2.3.5. *Immunofluorescence*

After sacrificed and processed of tissues, frozen slices were washed and blocked. After cultured with primary antibody overnight at 4 °C, the slices were further stained with FITC-conjugated secondary antibodies at room temperature for 2 h. After stained with 0.5 μg/mL of DAPI at room temperature for 5 min, sections were sealed by anti-fade mounting medium. Images were captured by a confocal microscope.

2.3.6. *Quantitative distribution in AD mice*

Ibu&FK@RNPs and Ibu&FK@NPs were intravenously injected into AD mice at the therapeutic dose, respectively. After 1, 2, 4 and 6 h, brains were collected and stored at −20 °C, and the plasma were collected immediately (Eppendorf, 5420, Germany) (1500×*g*, 10 min) for further study. 100 μL plasmas were mixed with 10 μL naproxen internal standard solution (25 μg/mL) and FK520 internal standard solution (2.5 μg/mL) for LC–MS/MS.

Brain was divided into hippocampus and normal tissues, and then 3 folds (*w/v*) of saline buffer were added for grinded thoroughly. 10 μL naproxen (500 ng/mL) and FK520 (50 ng/mL) were mixed with 100 μL tissue homogenate separately. After vortexed for 1 min, 200 μL zinc sulfate solution (0.2 mol/L) was added and vortex again. When finished, 400 μL acetonitrile were mixed for 2 min sonication. Then the samples were centrifuged for 10 min (13,000×*g*, 4 °C). The upper suspension was mixed with 1.5 mL ethyl acetate roughly and centrifuged for 10 min (13,000×*g*, 4 °C) to collect the upper organic layer. After dried by air and resuspended by 200 μL acetonitrile, the samples were collected for LC–MS/MS.

2.3.7. *Morris water maze test*

The AD model mice were randomly divided into five groups ($n = 5$). Wild-type C57BL/6 mice were used as healthy control. After 3 weeks of treatment, spatial sensitivity and learning memory ability of mice were assessed by the Morris water maze test. Mice were put in a round pool (100 cm in diameter and 50 cm in height), which contained a settled circle platform. If the mice found the platform within 60 s, they would have to stay for 10 s. If the mice couldn't find it, they would be guided to the platform for 10 s rest. After training for 5 days, the platform was removed and the spatial probe test was carried out. They were allowed to swim freely for 60 s. All data from tests were used for statistical analysis. After the test, all mice were sacrificed and the whole blood and plasma were gathered for complete blood counts (CBC) and blood biochemical test.

2.3.8. *Immunohistochemistry*

Ten-month-old double transgenic mice were divided into four groups on average ($n = 5$). The healthy control group was wild-type C57BL/6 mice. Medicinal preparation (Ibuprofen&FK506, Ibu&FK@NPs and Ibu&FK@RNPs) and PBS were administered intravenously every other day at the dose, including 1 mg/kg of FK506 and 16.5 mg/kg of ibuprofen. After 21 days, mice were sacrificed and their tissues (heart, liver, spleen, lung, kidney and brain) were sampled for H&E staining partly. In addition, the hippocampal slices were stained with toluidine blue solution to show the density of Nissl's body. The immunohistochemistry method was used to observe the concentration of Aβ plaques after sections were incubated by anti-A$\beta_{1\text{-}42}$ antibody.

2.3.9. *Evaluation of systemic toxicity*

The mice were weighed once every 2 days during the treatment. The cumulative toxicity of the nanoparticles was observed by H&E staining on the visceral slices of mice after treatment.

2.3.10. *Statistical analysis*

The paired Student's *t*-test was used in the comparative analysis of each group. $^{*}P < 0.05$, $^{**}P < 0.01$ and $^{***}P < 0.001$ are considered a statistically significant difference, respectively, and ns means not significant.

3. Results and discussion

3.1. *Synthesis and characterization of nanoparticles*

Firstly, the ROS-sensitive polymer (PEP) was obtained according to the synthetic routes (Fig. 2A). Then RAP was decorated in the PEG-terminals of PEP to form the RAGE-targeted polymer (PEPR). Intermediate products were characterized by ^{1}H NMR spectrum (Supporting Information Fig. S1) and MALDI-TOF MS (Supporting Information Fig. S2), respectively. Finally, PCL-MPEG, PEPR and drugs were mixed proportionally, and then self-assembled to prepare nanoparticles by the solvent diffusion method.

According to the bEnd.3 and PC12 cell viabilities by MTT assay (Supporting Information Fig. S3), cells were pre-incubated with 20 μmol/L Aβ oligomers for 12 h to simulate the pathological condition of AD[34,35,37]. Based on the bEnd.3 cell uptake efficiencies, Cou6@R$_1$NPs performed the best, which was 1.42 times higher than Cou6@NPs (Supporting Information Fig. S4). Therefore, RNPs with 6.7% RAP modification was used in the following experiments. The hydrodynamic diameter and zeta potential of Ibu&FK@RNPs were 86.87 nm and −38.31 mV, respectively (Supporting Information Table S2). The drug-loading capacity and encapsulation efficiency of ibuprofen were 60.48% and 4.24%, with those of FK506 were 55.56% and 6.79%,

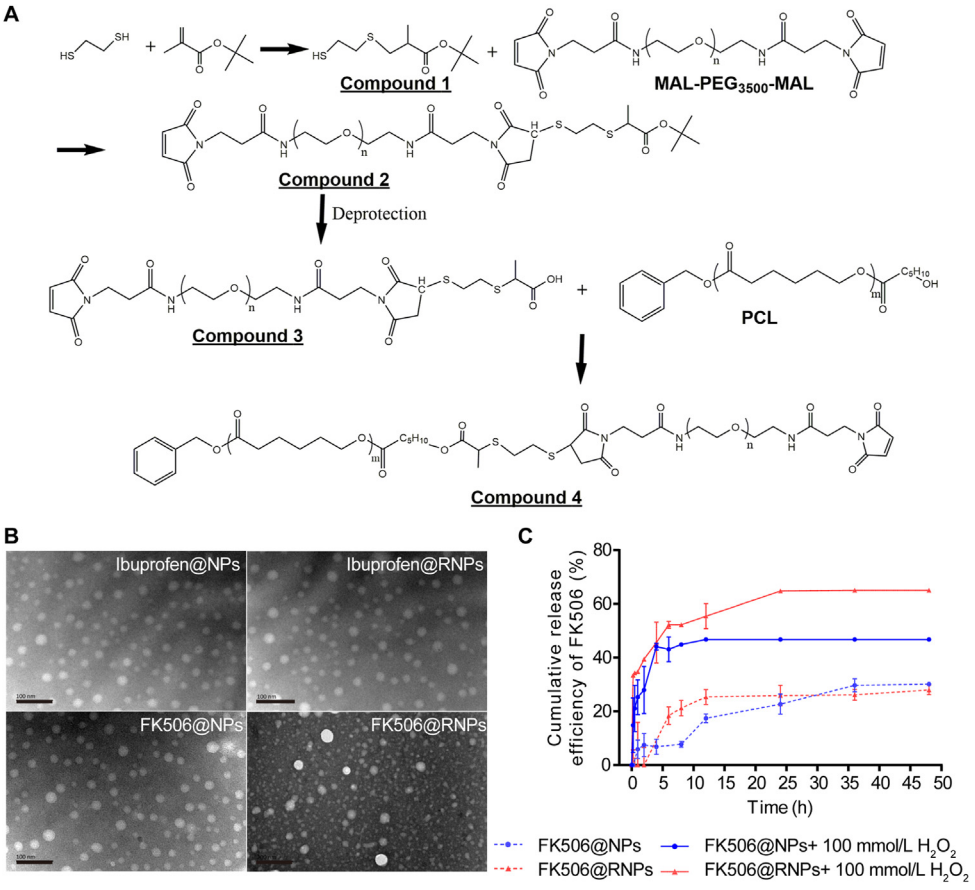

Figure 2 Synthetic routes and characterization of nanoparticles. (A) Synthetic routes of PEP. Compound **1**: EDT-MAA; compound **2**: MAL-PEG-EDT-MAA; compound **3**: MAL-PEG-MAL-EDT-MAH; compound **4**: PEP. (B) TEM images of nanoparticles. Scale bars represent 100 nm. (C) Cumulative release efficiency of FK506-loaded nanoparticles incubated in different solutions. Data are presented as mean ± SD (n = 3).

respectively. Transmission electronic microscopy (TEM) demonstrated spherical morphology of nanoparticles with a uniform dispersity and the diameter of Ibu&FK@RNPs was about 20 nm (Fig. 2B).

3.2. *Stability, drug release and cytotoxicity of Ibu&FK@RNPs*

An excellent stability of nanoparticles incubated in PBS and plasma is required to ensure their stable condition before and after administration[48]. After incubated in water or PBS for 48 h, there were no changes in the hydrodynamic diameters and PDI (Supporting Information Fig. S5). However, after 12 h incubation with 10% and 50% fetal bovine serum (FBS), their hydrodynamic diameters increased 30−60 nm and 50−60 nm, respectively, along with stable PDI. The reasons for above results might include the electrostatic repulsion[49] and formation of nanoparticle corona[50,51]. Therefore, the nanoparticles can be stored in water and PBS buffer for at least 48 h.

The cumulative release rate of FK506@RNPs in different solutions was measured by dialysis bags method (Fig. 2C)[52]. The 48 h cumulative FK506 release of nanoparticles in 100 mmol/L H_2O_2 solution was 45%−60%, while that in PBS was 20%−30%. The results show FK506 release was ROS-responsive.

According to the results of previous researches, the intravenous dose of 1 mg/kg of FK506 or 16.5 mg/kg of ibuprofen, equal to 50 μg/L of FK506 and 825 μg/L of ibuprofen in cells, might be effective to treat AD[24,53]. Cytotoxicity by MTT assays was measured to study the safety of Ibu&FK@RNPs (Fig. 3A and B, and Supporting Information Fig. S6). The results showed the cell viabilities of Ibu&FK@NPs and Ibu&FK@RNPs were about 100% and 97% respectively, indicating the good biosafety at treatment dose.

3.3. *Evaluation of in vitro cellular uptake and BBB transcytosis*

The bEnd.3 cell was pre-incubated with Aβ to simulate diseased BBB. The 2 h bEnd.3 cell internalization of Cou6-labeled nanoparticles was quantitatively analyzed by flow cytometry and imaged by confocal imaging (Fig. 3C and D). The cellular uptake of Cou6@RNPs was 1.42 times higher than Cou6@NPs in diseased bEnd.3 cells, while there was no difference in healthy cells. This result was consistent with corresponding confocal images, proving that RAP promoted internalization of nanoparticles specifically by the diseased cerebral vascular endothelial cell, but it did not work in normal state. Further, the inhibitor of RAGE, FPS-ZM1 was used to study the mechanism of RAP targeting (Supporting Information Fig. S7). Pre-incubated with FPS-ZM1 in diseased PC12 cells, the cellular uptake of Cou6@RNPs was 1.36 times lower than that without inhibitors, while there was no difference in the Cou6@RNPs group. The results dedicate that the enhanced cellular uptake of RAP-modified nanoparticles was ascribed to targeting RAGE.

On the other hand, the bEnd.3 monolayer pre-incubated Aβ was established to determine transportation of RNPs across the

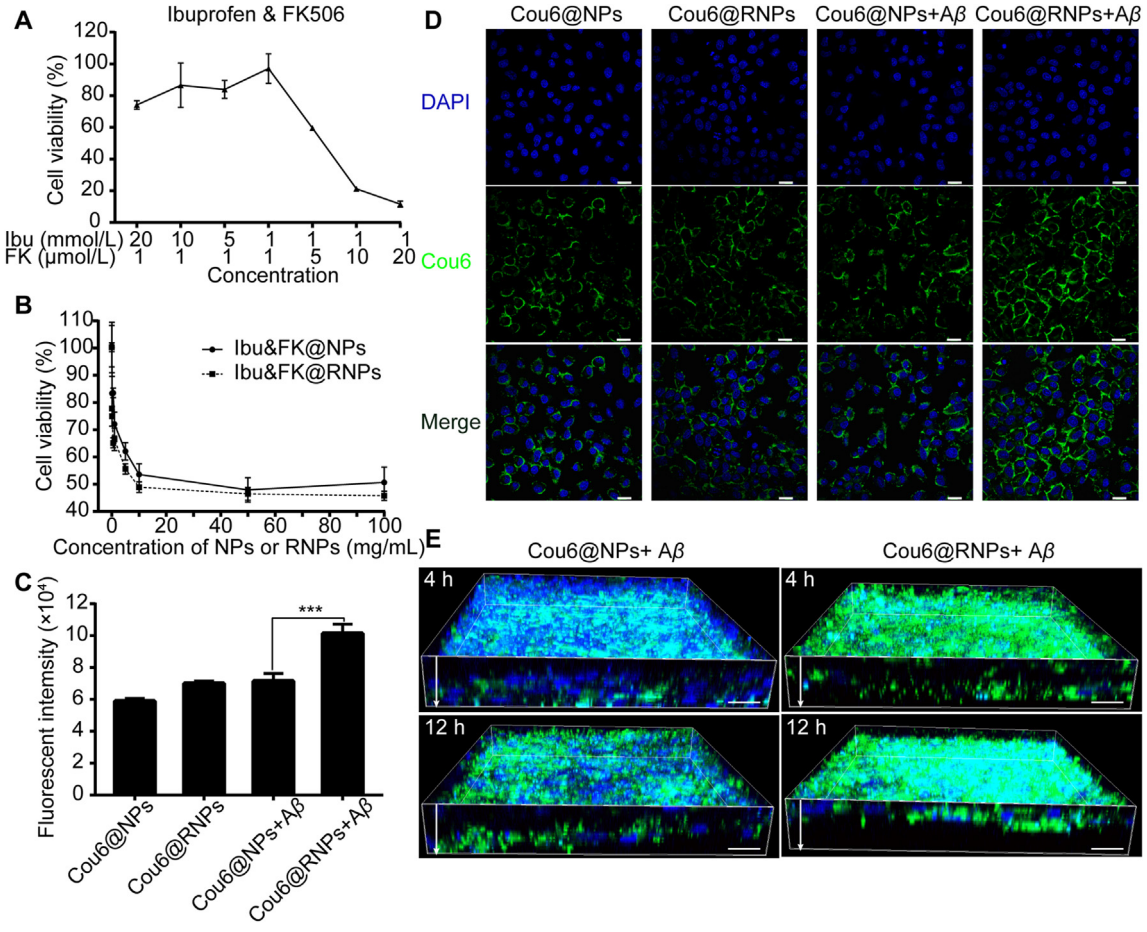

Figure 3 Intracellular behavioral studies. (A) The Aβ pre-incubated bEnd.3 cell viability of ibuprofen and FK506 measured by MTT assay. Data are presented as mean ± SD (n = 3). (B) The Aβ pre-incubated bEnd.3 cell viability of nanoparticles measured by MTT assay. Data are presented as mean ± SD (n = 3). (C) Quantitative uptake of nanoparticles incubated in bEnd.3 cells for 2 h. Data are presented as mean ± SD (n = 3). (D) Confocal fluorescence images of nanoparticles internalized by bEnd.3 cells. Scale bar represents 20 μm. (E) 3D confocal images of bEnd.3 monolayers in the donor chamber of transwell model after the introduction of different nanoparticles for 4 and 12 h. Scale bar represents 10 μm.

diseased BBB. After bEnd.3 cells seeded, the transmembrane resistance of monolayers was measured by a resistor every day[54]. Until Day 10, transmembrane resistance was stable at about 170 Ω, and then cells were incubated with 20 μmol/L Aβ oligomers for 12 h to simulate the diseased BBB. Then different Cou6-labeled nanoparticles were added into donor chamber of transwells and illustrated their transmembrane efficiency in 3D confocal images (Fig. 3E). The longitudinal (Z-axis) illustrated that Cou6@RNPs penetrated faster and deeper than control nanoparticles. The 4 h penetration depth of RNPs is much deeper than NPs in 12 h, indicating that RNPs had better diseased BBB transcytosis than controlled nanoparticles. This finding demonstrates the superiority of RAP modification in the diseased BBB penetration.

3.4. *In vivo distribution of RNPs*

To explore the *in vivo* BBB transcytosis and brain accumulation of nanoparticles in AD, the Cy5.5-labeled ibuprofen (Cy5.5-Ibu) was synthesized and demonstrated by ^{1}H NMR spectrum (Supporting Information Fig. S8). And then the biodistribution of Cy5.5-Ibu-labeled nanoparticles in AD mice were monitored by living imaging (Fig. 4A). As living images illustrated, the brain fluorescent intensity of mice administrated Cy5.5-Ibu@RNPs was continuously enhanced and increased to the top between 4 and 6 h, while there were no obvious changes in NPs group. After being administrated for 6 h, mice were sacrificed and *ex vivo* images of main organs were obtained (Fig. 4B and Supporting Information Fig. S9A). Although high level of nanoparticles was distributed in livers, the brain fluorescence intensity of RNPs group was much stronger than NPs group, which was 1.55 times higher according to semi-quantification (Fig. 4C). The results demonstrated that RAP modification endowed faster BBB transportation and more brain accumulation of nanoparticles in AD mice.

Brains were also sliced to observe the accumulation of nanoparticles and immunofluorescence colocation with RAGE by confocal imaging (Fig. 4D). The brain fluorescence intensity of Cy5.5-Ibu in RNPs group was much stronger than NPs group, and the obvious RAGE immunofluorescence images colocation was observed in RAP-modified nanoparticles. Moreover, there were no obvious differences of distribution in peripheral organs between RNPs and NPs, with similar findings illustrated in the confocal images of organs frozen slices (Supporting Information Fig. S9B and C). These results indicate that RAP modification could

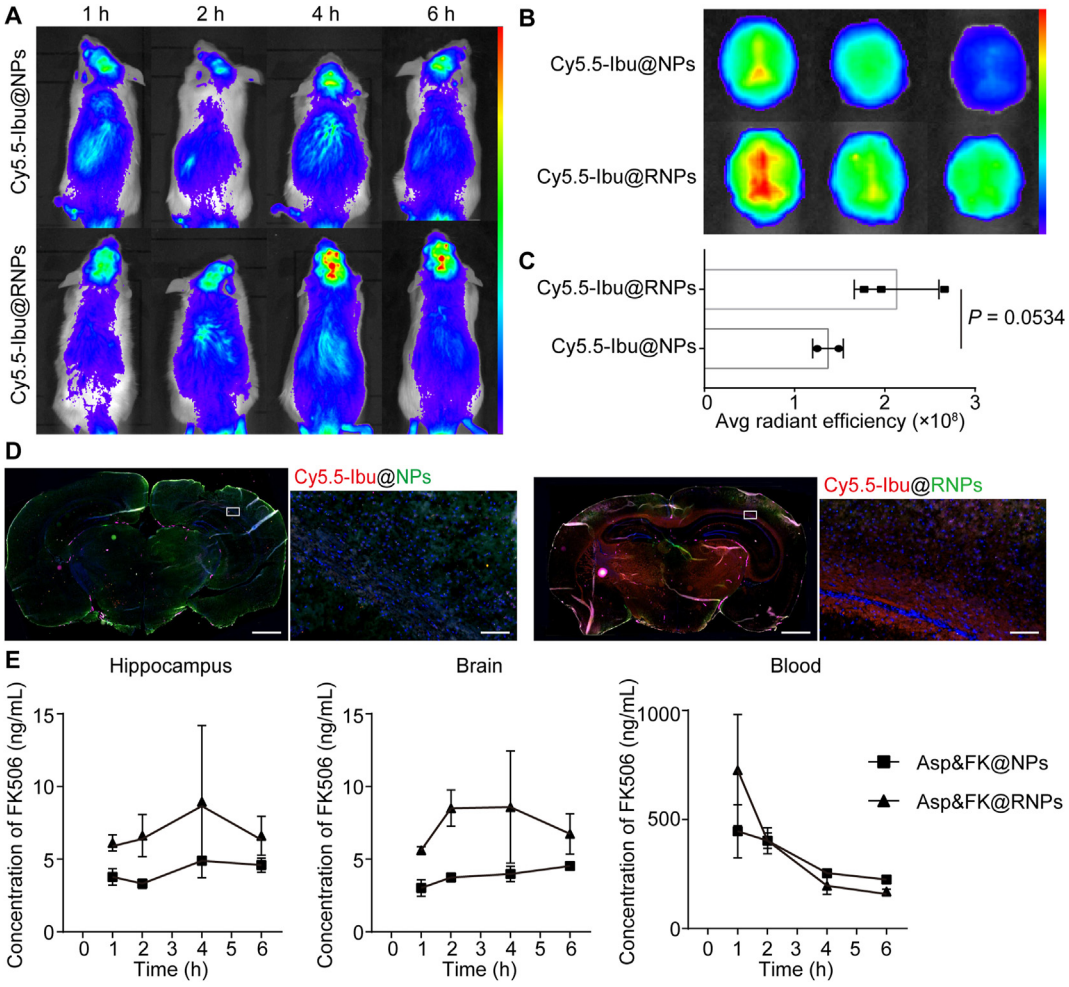

Figure 4 *In vivo* distribution of nanoparticles in AD mice. (A) Living imaging depicting the *in vivo* distribution of different formulations at different time. (B) *Ex vivo* imaging of brains in different groups after 6 h. (C) The semiquantitative fluorescence intensity of (B). Data were presented as mean ± SD (n = 3). (D) Representative confocal images of brains showing the accumulation of different nanoparticles and immunofluorescence colocation with RAGE. Blue: nuclei stained by DAPI, green: FITC-PEG-PCL, red: the positive rate of RAGE expression, pink: Cy5.5-Ibu. Scale bars represent 100 and 10 μm, respectively. (E) The *in vivo* concentration–time curves of FK506 measured by LC–MS/MS analysis.

improve the BBB transportation and facilitate brain accumulation of nanoparticles by targeted RAGE.

3.5. The in vivo concentration-time curves of FK506 and ibuprofen

After 1, 2, 4 and 4 h treatment, the concentration of drugs in blood was gradually decreased (Fig. 4E and Supporting Information Fig. S10). In the hippocampus and brain, concentration of FK506 was gradually raised to the top in 4 h. Besides, RAP peptide-modified nanoparticles had higher drug concentration in brain, indicating the peptide modification could improve the brain and AD targeting delivery capacity. However, the concentration–time curves of ibuprofen showed different trend which could be explained by its faster metabolism.

3.6. The behavioral test by Morris water maze

Progressive cognitive dysfunction and impaired behavior are typical clinical symptoms of AD[2], so Morris Water maze test is often used to assess the behavioral conditions in animal experiment. During training, the average time spent to reach the platform of mice administrated PBS, Ibuprofen&FK506 and Ibu&FK@NPs were fluctuating and irregular (Fig. 5A). However, the above condition did not appear in the Ibu&FK@RNPs group whose average incubation period to reach the platform was gradually shortened and similar to healthy mice, which implied strong learning and memory abilities. After the training was completed, spatial probe test was experimented with the original platform removed (Fig. 5B and Supporting Information Fig. S11). In the placed navigation test, representative swimming paths of AD mice showed aimless circles in PBS and Ibuprofen&FK506 groups. In contrast, the swimming paths of Ibu&FK@RNPs group and healthy mice were purposeful in searching for the platform and concentrated in the target quadrant. In addition, time spent to reach the platform was also presented statistically different (Fig. 5C). Compared with the mice treated by PBS (39.6 ± 18.3 s), Ibuprofen&FK506 (27.2 ± 12.7 s) and Ibu&FK@NPs (31.7 ± 9.1 s), the AD mice administrated with Ibu&FK@RNPs took the least time (10.2 ± 5.2 s) to reach the platform, which was similar to healthy mice (11.9 ± 4.4 s). The frequencies of mice passing through the location of original

platform were also counted (Fig. 5D). The AD mice treated with PBS passed through the platform for less than once, while Ibuprofen&FK506 (2.2 ± 1.1 times) or Ibu&FK@NPs (2.2 ± 1.2 times) groups increased, respectively. Besides, compared with healthy mice (4.0 ± 1.7 times), the Ibu&FK@RNPs group showed similar frequency (4.3 ± 1.2 times). These results suggested the sense of space in AD mice could be improved by Ibu&FK@RNPs and reflected the RAGE targeted drug depot significantly improved the intracerebral drug delivery and ameliorated learning acquisition and the sense of space of AD.

3.7. *Decrease of the production of β amyloid plaques in vivo*

Although all Aβ targeted medicines were terminated, Aβ plaques were still recognized as the characteristic physiological marker of AD[5]. Immunohistochemical staining was used to illustrate the amount of Aβ plaques in the hippocampus of APP/PS1 mice (Fig. 5E). We observed many and large plaques, illustrating Aβ plaques were overexpressed in the brain of APP/PS1 mice. Excitingly, the Aβ plaques burden was significantly reduced by 1.64 times after the treatment of Ibu&FK@RNPs and there was no statistic difference in combination drug treatment (Fig. 5F). This result indicates the combination medication could specifically inhibit the production of toxic isoform Aβ plaques. However, the modification of nanocarriers had few efficacies in reducing Aβ plaques.

3.8. *Neuroprotective effects*

In AD, Aβ plaques and tau tangles work together to increase intracellular concentration of Ca^{2+} and induce neurotoxicity[22]. Thus, we evaluated the function of neurons by Nissl staining (Fig. 6A and B). We chose to evaluate the CA1 area because it was prone to be damaged in the hippocampus. The marked neuronal damages, including neuronal hypocellularity, were observed in the CA1 hippocampus of the APP/PS1 mice treated with PBS, Ibuprofen&FK506 and Ibu&FK@NPs. Nevertheless, the above phenomena were not found in healthy

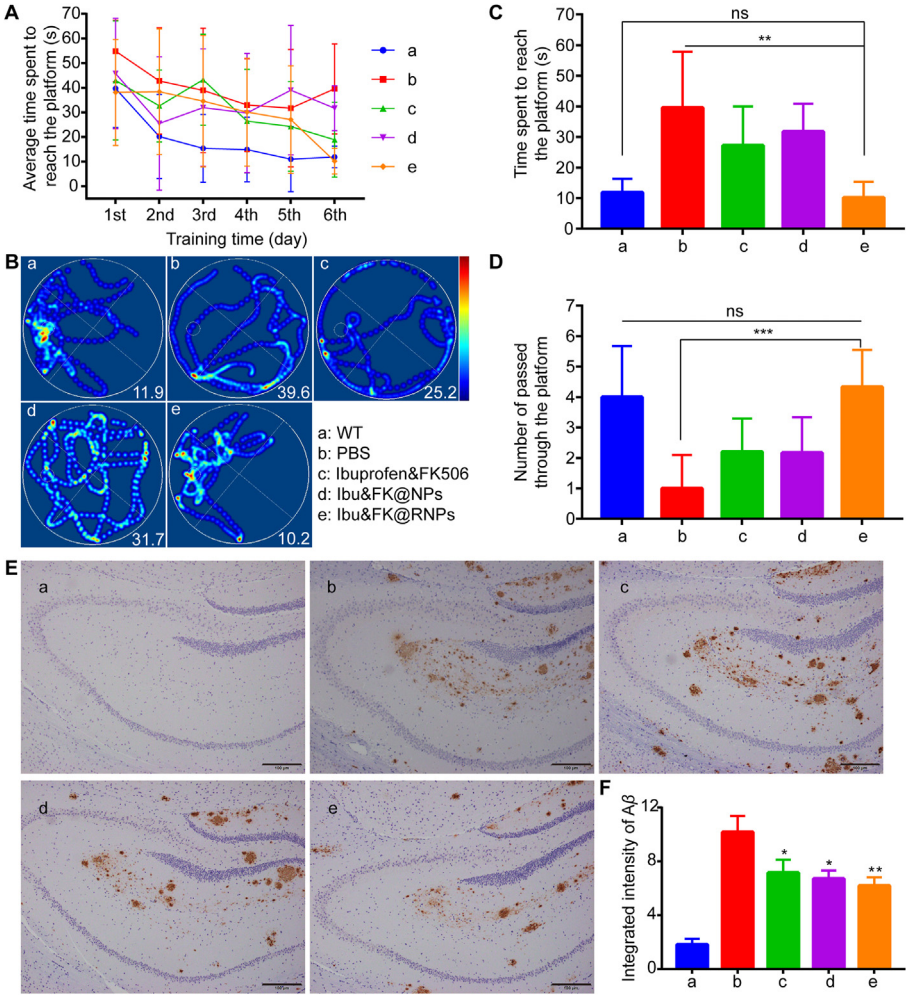

Figure 5 Learning acquisition and Aβ plaques reduction. (A) Average time to reach the platform in the training process of AD mice in Morris water maze test. Data are presented as mean ± SD (n = 5). (B) The representative swimming paths of AD mice in Morris water maze test, numbers in the lower right indicate the average time spent to reach the platform. (C) The time for mice to reach the platform of AD mice in the Morris water maze test. Data are presented as mean ± SD (n = 5). (D) The frequency for the AD mice passing through the platform in the spatial probe test. Data are presented as mean ± SD (n = 5). (E) Representative images of amyloid plaques stained by immunohistochemical in hippocampus from APP/PS1 transgenic mice. Scale bar represents 100 μm. (F) The semiquantitative integrated intensity of Aβ plaques by immunohistochemical staining in APP/PS1 transgenic mice. Data are presented as mean ± SD (n = 3).

mice and Ibu&FK@RNPs groups. Besides, the quantitative expression of Nissl's body in the CA1 area showed that the quantitative in Ibu&FK@RNPs group was 3 times higher than that of APP/PS1 mice. These results demonstrated that RAP-modified formulations attenuated the impairment of neuronal integrity as well as neuron loss. Additionally, new neurons could continue to be generated throughout the adulthood of healthy mammals and the nerve regeneration might be promoted by FK506[21,25]. In consequence, the synaptic change of neuron skeleton protein (MAP2) is usually used to monitor the neurite outgrowth and provide a subtler indication of neuronal function[55]. From the immunofluorescence of MAP2, hippocampus of APP/PS1 mice, Ibuprofen&FK506 and Ibu&FK@RNPs groups showed decreased MAP2 expression, while healthy mice and the Ibu&FK@RNPs group had more positive expression of MAP2 (Fig. 6C and D). Accordingly, Ibu&FK@RNPs could not only effectively protect the neurons, but also increase the number of synapses to ameliorate the memory decline.

3.9. *Anti-neuroinflammatory effects*

The active neuroinflammatory responses in the AD brain were manifested by excessive activation of glial cells and over-expression of inflammatory factors[47]. The immunofluorescence images of glial fibrillary acidic protein (GFAP) showed dendroid chunks spreading among the cerebral cortex of APP/PS1 mice and Ibuprofen&FK506 groups, illustrating the over-activated astrocytes of AD (Fig. 7A and Supporting Information Fig. S12A). The inhibited status of astrocytes was demonstrated by the small strip and spotty fluorescence signals of GFAP which was showed in Ibu&FK@RNPs group and healthy mice. The quantification of GFAP in the cerebral cortex of mice showed 12.78 times lower level than that of APP/PS1 mice. The results proved the excessive activation of astrocytes was significantly inhibited by Ibu&FK@RNPs.

In AD pathology, the NF-κB pathway of astrocytes plays an essential role in the vicious circle of neuroinflammatory response and neuronal dysfunction[56]. To explore this pathway, we studied the expression of NF-κB and associated inflammatory factors (IL-1β) in brains. The results of Western blot showed the expression of NF-κB was significantly increased in APP/PS1 mice in comparison with control groups (Fig. 7B). Besides, after treated with Ibu&FK@RNPs, the expression of NF-κB was similar to healthy mice. The relative content of NF-κB in Ibu&FK@RNPs group was 1.57 times lower than APP/PS1 mice, but showed no statistical significance comparing with healthy mice (Fig. 7C). In addition, there were no differences with APP/PS1 mice between Ibuprofen&FK506 and Ibu&FK@NPs groups. Additionally, we also measured the level of IκBα in the brain by Western Blot (Supporting Information Fig. S13). The semiquantitative integrated intensity of IκBα in Ibu&FK@RNPs group was 1.79 times

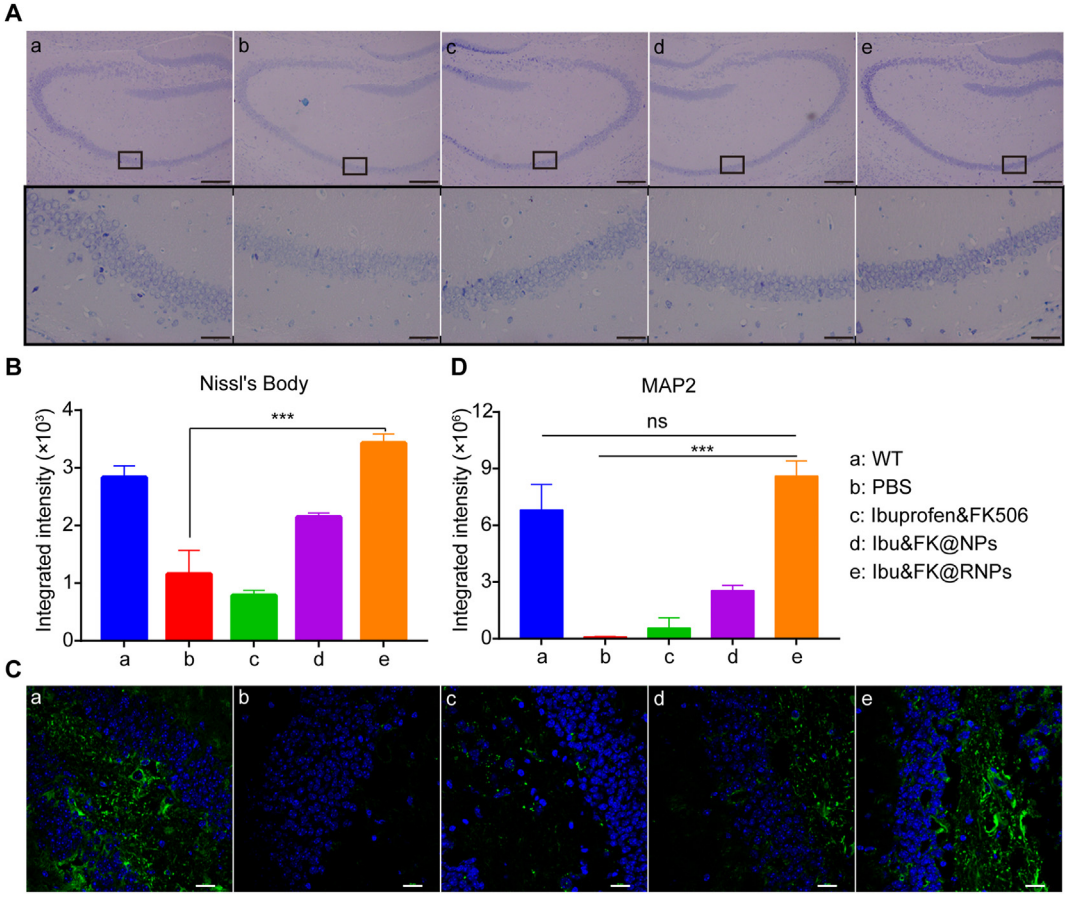

Figure 6 Neuroprotective effects in APP/PS1 mice. (A) Nissl staining in the hippocampus. The black box shows the hippocampal CA1 area. Scale bars represent 100 and 10 μm, respectively. (B) Quantitative expression of Nissl's body in the CA1 area. (C) Immunofluorescence of MAP2 in the hippocampus. Green represents the positive rate of MAP2 expression, blue represents nuclei stained by DAPI and scale bar represents 20 μm. (D) Quantification of MAP2 in the hippocampus of mice in different treatment groups. Data are presented as mean ± SD (n = 3).

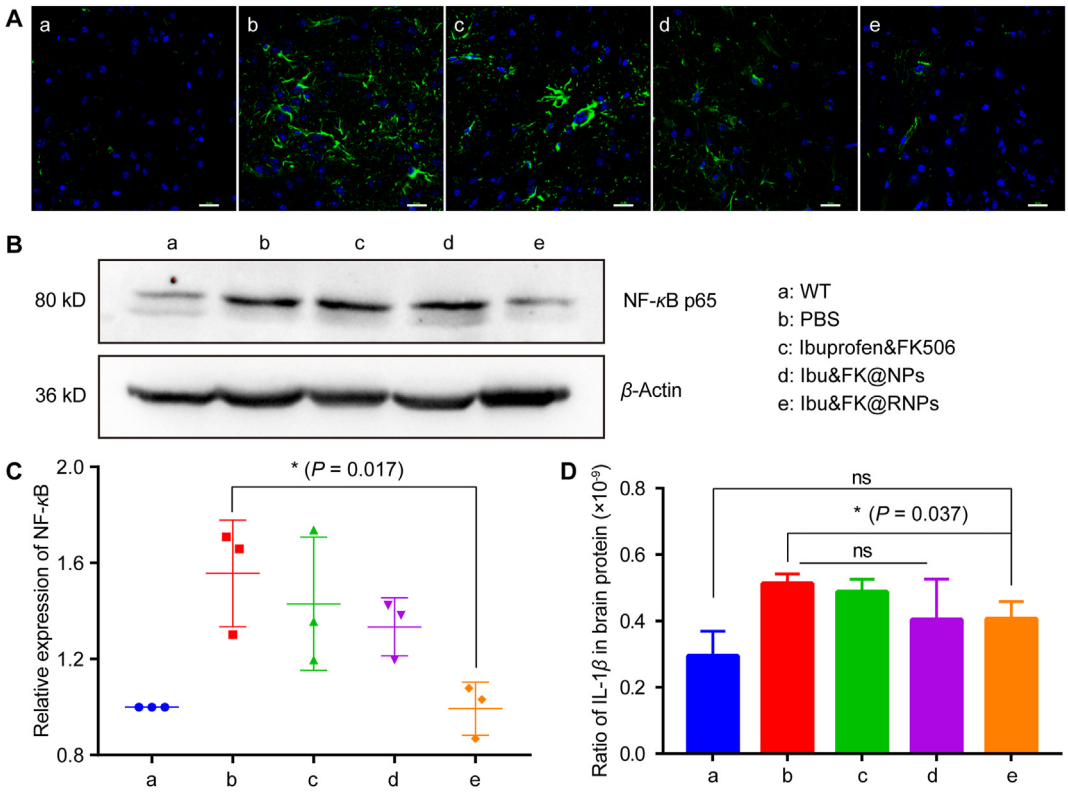

Figure 7 Anti-neuroinflammatory effects in APP/PS1 mice. (A) Immunofluorescence of GFAP in the cerebral cortex. Green represented the positive rate of GFAP expression, blue represented nuclei stained by DAPI and scale bar represents 20 μm. (B) Western Blot of NF-κB in the brain. (C) The semiquantitative integrated intensity of NF-κB by Western Blot. Data are presented as mean ± SD ($n = 3$). (D) The proportion of IL-1β in the brain proteins. Data are presented as mean ± SD ($n = 3$).

lower than that of APP/PS1 mice, dedicating that drugs could inhibit the upstream signal of NF-κB pathway to anti-neuroinflammation.

IL-1β was an important inflammatory factor of NF-κB pathway, so we also measured its concentration by ELISA assays (Fig. 7D and Fig. S12B). The results show the concentration of IL-1β was increased by 6.73 and 1.74 times in serum and brain separately, indicating the over-expression of IL-1β in AD. Moreover, the serum and brain concentration of IL-1β in Ibu&FK@RNPs group was 4.59 and 1.26 times lower than APP/PS1 mice, respectively. In serum, there were similar anti-inflammatory effects between Ibu&FK@RNPs and control formulations. Surprisingly, there was evident significance in brain level of IL-1β between Ibu&FK@RNPs and control formulations, demonstrating the improvement of anti-neuroinflammatory effects by RAP-modified nanoparticles.

As supplementary, we performed routine blood tests on the mice (Supporting Information Fig. S14). Typical inflammatory indicators, including the number of WBC, LY and PMN, were elevated in APP/PS1 mice, indicating peripheral inflammation of AD. Furthermore, this condition was dampened by medicine, in accordance with the peripheral expression of IL-1β. These findings demonstrate that Ibu&FK@RNPs can inhibit NF-κB pathway for anti-neuroinflammation, and thus it can treat AD efficiently.

3.10. Evaluation of systemic toxicity

In vivo toxicity of the nanoparticles was evaluated by body weight changes, organs' H&E staining and related biochemical indicators. Firstly, APP/PS1 mice were administrated different formulations and their body weights were recorded every 2 days. The results show that there was no obvious difference among all groups (Supporting Information Fig. S15). After 21 days of treatment, mice were sacrificed and their blood samples were prepared. Blood biochemical indexes showed that ALT, AST and BUN were all within the normal range (Supporting Information Table S2). Besides, the H&E staining of organs proved there were no visible pathological changes in each groups (Supporting Information Fig. S16). Therefore, the RAGE-targeting drug delivery depot possessed excellent safety.

4. Conclusions

In this study, we designed an ROS-sensitive and RAGE targeted drug delivery depot (Ibu&FK@RNPs), which could progressively target diseased BBB and brain parenchymal cells to improve the treatment of ibuprofen and FK506 against AD. At first, cellular uptake efficiency validated that RAP could specifically recognize the RAGE on diseased BBB and improve the internalization of nanoparticles by CMT. Besides, the *in vitro* cumulative release of FK506@RNPs incubated in 100 mmol/L H_2O_2 solutions proved the ROS-responsive drug release of nanoparticles. Secondly, *in vitro* diseased BBB transcytosis and *in vivo* fluorescence imaging investigation demonstrated that RAP-modified nanoparticles could pass through BBB and target the lesion site more quickly and effectively. Finally, the results of Morris water maze test and immunohistochemistry displayed that Ibu&FK@RNPs inhibited the production of Aβ and improved the dementia symptoms. As a result, Ibu&FK@RNPs

significantly reduced the neurological damage and suppressed neuroinflammation in AD mice. Furthermore, this ROS-sensitive and RAGE targeted drug delivery system could be adopted to enhance the therapeutic efficacy for other brain diseases.

Acknowledgements

The work was supported by National Natural Science Foundation of China (81872806, 81961138009), 111 Project (B18035, China), the Fundamental of Research Funds for the Central Universities (China), the Open Research Fund of Chengdu University of Traditional Chinese Medicine and the Open Research Fund of Chengdu University of Traditional Chinese Medicine State Key Laboratory of Characteristic Chinese Medicine Resources in Southwest China.

Author contributions

Huile Gao and Xueqin He conceived and administered the project. Xueqin He, Xiaorong Wang, Lianyi Yang, Zhihang Yang and Yazhen Wang conducted the investigation. Xueqin He, Xiaorong Wang and Lianyi Yang performed experiments. Huile Gao applied for the funding. Xueqin He, Wenqi Yu, Meiwan Chen, Rui Liu and Huile Gao wrote the manuscript. All of the authors have read and approved the final manuscript.

Conflicts of interest

The authors declare no conflicts of interest.

Appendix A. Supporting information

Supporting data to this article can be found online at https://doi.org/10.1016/j.apsb.2022.02.001.

References

1. Scheltens P, Blennow K, Mbbreteler M, Destrooper B, Bfrisoni G, Salloway S, et al. Alzheimer's disease. *Lancet* 2016;**388**:505−17.
2. Alzheimer's Disease International. *World Alzheimer report 2018*. 2018. Available from: https://www.alzint.org/resource/world-alzheimer-report-2018/.
3. Akent S, Lspires-jones T, Sdurrant C. The physiological roles of tau and Aβ: implications for Alzheimer's disease pathology and therapeutics. *Acta Neuropathol* 2020;**140**:417−47.
4. Gcanter R, Penney J, Tsai LH. The road to restoring neural circuits for the treatment of Alzheimer's disease. *Nature* 2016;**539**:187−96.
5. Cummings J, Lee G, Ritter A, Sabbagh M, Zhong K. Alzheimer's disease drug development pipeline: 2020. *Alzheimer Dement Transl Res Clin Interv* 2020;**6**:1−29.
6. Bradburn S, Murgatroyd C, Ray N. Neuroinflammation in mild cognitive impairment and Alzheimer's disease: a meta-analysis. *Ageing Res Rev* 2019;**50**:1−8.
7. Leng F, Edison P. Neuroinflammation and microglial activation in Alzheimer disease: where do we go from here? *Nat Rev Neurol* 2020;**17**:157−72.
8. Calsolaro V, Edison P. Neuroinflammation in Alzheimer's disease: current evidence and future directions. *Alzheimers Dement* 2016;**12**:719−32.
9. Hmoore A, Ko'banion M. Neuroinflammation and anti-inflammatory therapy for Alzheimer's disease. *Adv Drug Deliv Rev* 2002;**54**:1627−56.
10. Leal F, Hannah S, Ingav H, Rebecca B, Dietmar R, Eicke L, et al. β-Amyloid clustering around ASC fibrils boosts its toxicity in microglia. *Cell Rep* 2020;**30**:3743−54.
11. Chen CH, Zhou WH, Liu SC, Deng Y, Cai F, Tone M, et al. Increased NF-κB signalling up-regulates BACE1 expression and its therapeutic potential in Alzheimer's disease. *Int J Neuropsychoph* 2011;**15**:77−90.
12. Bindu S, Mazumder S, Dey S, Pal C, Goyal M, Alam A, et al. Nonsteroidal anti-inflammatory drug induces proinflammatory damage in gastric mucosa through NF-κB activation and neutrophil infiltration: anti-inflammatory role of heme oxygenase-1 against nonsteroidal anti-inflammatory drug. *Free Radical Bio Med* 2013;**65**:456−67.
13. Mladenova D, Pangon L, Currey N, Ng I, Amusgrove E, Tgrey S, et al. Sulindac activates NF-κB signaling in colon cancer cells. *Cell Commun Signal* 2013;**65**:456−67.
14. Rwbrady R, Jloveridge C, Gdunlop M, Astark L. C-Src dependency of NSAID-induced effects on NF-κB-mediated apoptosis in colorectal cancer cells. *Carcinogenesis* 2011;**32**:1069−77.
15. Chattopadhyay M, Goswami S, Brodes D, Kodela R, Avelazquez C, Boring D, et al. NO-releasing NSAIDs suppress NF-κB signaling *in vitro* and *in vivo* through *S*-nitrosylation. *Cancer Lett* 2010;**298**:204−11.
16. Chen JY, Stark L. Aspirin prevention of colorectal cancer: focus on NF-κB signalling and the nucleolus. *Biomedicines* 2017;**5**:43.
17. Ghanghas P, Jain S, Rana CD, Nsanyal S. Chemopreventive action of non-steroidal anti-inflammatory drugs on the inflammatory pathways in colon cancer. *Biomed Pharmacother* 2016;**78**:239−47.
18. Lim GP, Yang F, Chu T, Chen P, Beech W, Teter B, et al. Ibuprofen suppresses plaque pathology and inflammation in a mouse model for Alzheimer's disease. *J Neurosci* 2000;**20**:5709−14.
19. Lim GP, Yang F, Chu T, Gahtan E, Ubeda O, Beech W, et al. Ibuprofen effects on Alzheimer pathology and open field activity in APPsw transgenic mice. *Neurobiol Aging* 2001;**22**:983−91.
20. Annc MK, Isabel C, Lokman H, Hoon R, Williaml K, Salvatore O, et al. Ibuprofen reduces Aβ, hyperphosphorylated tau and memory deficits in Alzheimer mice. *Brain Res* 2008;**1207**:225−36.
21. Anete R, Bradleyt H, Taral SJ. Calcineurin inhibition with FK506 ameliorates dendritic spine density deficits in plaque-bearing Alzheimer model mice. *Neurobiol Dis* 2011;**41**:650−4.
22. Frankm LF. Calcium dyshomeostasis and intracellular signalling in Alzheimer's disease. *Nat Rev Neurosci* 2002;**3**:862−72.
23. Jerela F, Cassia O, Anthony A, Jazmin F, Michael M, Andrea P, et al. Neuroprotective effects of the immunomodulatory drug FK506 in a model of HIV1-gp120 neurotoxicity. *J Neuroinflamm* 2016;**1**:120.
24. Ding L, Nan WH, Zhu XB, Li XM, Zhou LY, Chen HJ, et al. Rapamycin and FK506 derivative TH2849 could ameliorate neurodegenerative diseases through autophagy with low immunosuppressive effect. *CNS Neurosci Ther* 2018;**25**:452−64.
25. Kasra T, Chan K, Mollys S, Tessa G, Gregoryh B. Local delivery of FK506 to injured peripheral nerve enhances axon regeneration after surgical nerve repair in rats. *Acta Biomater* 2019;**96**:211−21.
26. Aoneal M, Rstallings N, Smalter J. Alzheimer's disease, dendritic spines, and calcineurin inhibitors: a new approach? *ACS Chem Neurosci* 2018;**9**:1233−4.
27. Ruan SB, Zhou Y, Jiang XG, Gao HL. Rethinking CRITID procedure of brain targeting drug delivery: circulation, blood brain barrier recognition, intracellular transport, diseased cell targeting, internalization, and drug release. *Adv Sci* 2021;**8**:2004025.
28. Gao HL. Progress and perspectives on targeting nanoparticles for brain drug delivery. *Acta Pharm Sin B* 2016;**4**:18−36.
29. Gao HL. Perspectives on dual targeting delivery systems for brain tumors. *J Neuroimmune Pharm* 2017;**12**:6−16.
30. Ruan SB, Qin L, Xiao W, Hu C, Zhou Y, Wang RR, et al. Acid-responsive transferrin dissociation and GLUT mediated exocytosis for increased blood–brain barrier transcytosis and programmed glioma targeting delivery. *Adv Funct Mater* 2018;**30**:1802227.
31. Cai LL, Yang CY, Jia WF, Liu YW, Xie R, Lei T, et al. Endo/lysosome-escapable delivery depot for improving BBB transcytosis and

neuron targeted therapy of Alzheimer's disease. *Adv Funct Mater* 2020;**27**:1909999.
32. Lei T, Yang ZH, Xia X, Chen YX, Yang XT, Xie R, et al. A nano-cleaner specifically penetrates the blood–brain barrier at lesions to clean toxic proteins and regulate inflammation in Alzheimer's disease. *Acta Pharm Sin B* 2021;**11**:4032−44.
33. Fritz G. RAGE: a single receptor fits multiple ligands. *Trends Biochem Sci* 2011;**36**:625−32.
34. Mruthinti S, Sood A, Humphrey CL, Swamy-Mruthinti S, Buccafusco JJ. The induction of surface β-amyloid binding proteins and enhanced cytotoxicity in cultured PC-12 and IMR-32 cells by advanced glycation end products. *Neuroscience* 2006;**142**:463−73.
35. Yan FL, Han GL, Wu GJ. Cytotoxic role of advanced glycation end-products in PC12 cells treated with betaamyloid peptide. *Mol Med Rep* 2013;**8**:367−72.
36. Yan FL, Zheng Y, Zhao FD. Effects of ginkgo biloba extract EGb761 on expression of RAGE and LRP-1 in cerebral microvascular endothelial cells under chronic hypoxia and hypoglycemia. *Acta Neuropathol* 2008;**116**:529−35.
37. Edonahue J, Lflaherty S, Ejohanson C, Aduncan J, Dsilverberg G, Cmiller M, et al. RAGE, LRP-1, and amyloid-beta protein in Alzheimer's disease. *Acta Neuropathol* 2006;**112**:405−15.
38. Thiruvengadam A, Vijaya R, Sobeydab G, Annm S, Craigd L. S100P-derived RAGE antagonistic peptide reduces tumor growth and metastasis. *Clin Cancer Res* 2012;**18**:4356−64.
39. Shi YG, Di S, Da LN, Miao RY, Kun Q, Wei Z, et al. Smart tumor microenvironment-responsive nanotheranostic agent for effective cancer therapy. *Adv Funct Mater* 2020;**30**:2000486.
40. Gulzar A, Xu JT, Wang C, He F, Yang D, Gai SL, et al. Tumour microenvironment responsive nanoconstructs for cancer theranostic. *Nano Today* 2019;**26**:16−56.
41. Song QL, Yin YJ, Shang LH, Wu TT, Zhang D, Kong M, et al. Tumor microenvironment responsive nanogel for the combinatorial antitumor effect of chemotherapy and immunotherapy. *Nano Lett* 2017;**17**:6366−75.
42. Lu YF, Guo ZY, Zhang YJ, Li C, Zhang Y, Guo Q, et al. Alzheimer's disease: microenvironment remodeling micelles for Alzheimer's disease therapy by early modulation of activated microglia (Adv. Sci. 4/2019). *Adv Sci* 2019;**6**:1970024.
43. Jinkwon H, Cha MY, Kim D, Kyukim D, Soh M, Shin K, et al. Mitochondria-targeting ceria nanoparticles as antioxidants for Alzheimer's disease. *ACS Nano* 2016;**10**:2860−70.
44. Wilson D, Dalmasso G, Wang LX, Sitaraman S, Merlin D, Murthy N. Orally delivered thioketal nanoparticles loaded with TNF-α−siRNA target inflammation and inhibit gene expression in the intestines. *Nat Mater* 2010;**9**:923−8.
45. Xu QH, He CL, Xiao CS, Chen XS. Reactive oxygen species (ROS) responsive polymers for biomedical applications. *Macromol Biosci* 2016;**16**:635−46.
46. Deng HZ, Zhao XF, Liu JJ, Deng LD, Zhang JH, Liu JF, et al. Reactive oxygen species (ROS) responsive PEG-PCL nanoparticles with pH-controlled negative-to-positive charge reversal for intracellular delivery of doxorubicin. *J Mater Chem B* 2015;**3**:9397−408.
47. Tang X, Sheng QL, Xu CQ, Li M, Rao JD, Wang XH, et al. PH/ATP cascade-responsive nano-courier with efficient tumor targeting and siRNA unloading for photothermal-immunotherapy. *Nano Today* 2021;**37**:101083.
48. Tphan H, Jhaes A. What does nanoparticle stability mean? *J Phys Chem C* 2019;**123**:16495−507.
49. Sano K, Igarashi N, Onumaarazoe Y, Ishida Y, Ebina Y, Sasaki T, et al. Internal structure and mechanical property of an anisotropic hydrogel with electrostatic repulsion between nanosheets. *Polymer* 2019;**177**:43−8.
50. Xiao W, Wang YZ, Zhang HL, Liu YW, Xie R, He XQ, et al. The protein corona hampers the transcytosis of transferrin-modified nanoparticles through blood−brain barrier and attenuates their targeting ability to brain tumor. *Biomaterials* 2021;**274**:120888.
51. Xiao W, Gao HL. The impact of protein corona on the behavior and targeting capability of nanoparticle-based delivery system. *Int J Pharmaceut* 2018;**1**−**2**:328−39.
52. Wang YQ, Li CJ, Du LB, Liu Y. A reactive oxygen species-responsive dendrimer with low cytotoxicity for efficient and targeted gene delivery. *Chin Chem Lett* 2020;**1**:275−80.
53. Laura G, Ennio O, Gary W. Non-steroidal anti-inflammatory drugs (NSAIDs) in Alzheimer's disease: old and new mechanisms of action. *J Neurochem* 2004;**91**:521−36.
54. Yang XT, Chen XC, Lei T, Qin L, Zhou Y, Hu C, et al. The construction of *in vitro* nasal cavity-mimic M-cell model, design of M cell-targeting nanoparticles and evaluation of mucosal vaccination by nasal administration. *Acta Pharm Sin B* 2020;**6**:1094−105.
55. Sánchez C, Díaz-nido J, Avila J. Phosphorylation of microtubule-associated protein 2 (MAP2) and its relevance for the regulation of the neuronal cytoskeleton function. *Prog Neurobiol* 2000;**61**:133−68.
56. Hong L, Alexandra L, Angieca C, Nadia A, Joannal J, Zheng H. Astrocyte-microglia cross talk through complement activation modulates amyloid pathology in mouse models of Alzheimer's disease. *J Neurosci* 2016;**36**:577.